

University of Heidelberg  
Department of Physics and Astronomy  
Institute for Theoretical Physics

BACHELOR THESIS IN PHYSICS

---

**Search for Invisible Decays of a  
Higgs Boson in Weak Boson Fusion  
and in Association with a Z Boson**

---

*submitted by*  
Rhea Penelope Moutafis  
born in Egling (Germany)

*Supervisor*  
Prof. Dr. Tilman Plehn

This bachelor thesis has been carried out by Rhea Moutafis  
at the Institute for Theoretical Physics in Heidelberg  
under the supervision of Prof. Dr. Tilman Plehn.

Heidelberg, June 05, 2017



## Abstract

The sensitivity of weak boson fusion and the associated  $ZH$  production in the search for invisible decays of a Higgs boson is compared at a total collider energy of 13 TeV. The signal and background events are produced with SHERPA and get passed through DELPHES. The signal and background are separated with a cut-and-count approach and with boosted decision trees. The boosted decision tree is found to improve the signal-to-background ratio in weak boson fusion by a factor of 3.1 and in associated  $ZH$  production by 37% in comparison to the cut-and-count approach. With a boosted decision tree, the signal-to-background ratios of the two channels agree within their uncertainties. However, the weak boson fusion is favoured as it is more sensitive to the available amount of data.

## Zusammenfassung

Die Eignung der schwachen Boson-Fusion und der assoziierten  $ZH$ -Produktion auf der Suche nach unsichtbaren Zerfällen eines Higgs-Bosons wird bei einer Kollisionsenergie von 13 TeV untersucht. Die Signal- und Hintergrund-Ereignisse werden mit SHERPA produziert und durchlaufen DELPHES. Signal und Hintergründe werden mit einem Cut-and-Count-Ansatz sowie mit Boosted Decision Trees getrennt. Der Boosted Decision Tree verbessert das Verhältnis von Signal zu Hintergrund in der schwachen Boson-Fusion um den Faktor 3,1 und in der assoziierten  $ZH$ -Produktion um 37%, verglichen mit dem Cut-and-Count-Ansatz. Mit einem Boosted Decision Tree stimmen die Signal-zu-Hintergrund-Verhältnisse innerhalb ihrer Fehlergrenzen überein. Allerdings ist die schwache Boson-Fusion bevorzugt, da sie stärker auf die vorhandene Datenmenge anspricht.



# Contents

<b>1</b>	<b>Introduction</b>	<b>1</b>
<b>2</b>	<b>Phenomenology</b>	<b>3</b>
2.1	Standard Model . . . . .	3
2.2	Collider Physics . . . . .	4
<b>3</b>	<b>Production Channels</b>	<b>10</b>
3.1	Weak Boson Fusion . . . . .	10
3.2	Associated $ZH$ Production . . . . .	13
3.3	Methods and Software . . . . .	17
<b>4</b>	<b>Results in Weak Boson Fusion</b>	<b>20</b>
4.1	Cut Flow . . . . .	20
4.2	Boosted Decision Trees . . . . .	23
<b>5</b>	<b>Results in Associated <math>ZH</math> Production</b>	<b>27</b>
5.1	Cut Flow . . . . .	27
5.2	Boosted Decision Trees . . . . .	30
<b>6</b>	<b>Comparison</b>	<b>33</b>
<b>7</b>	<b>Conclusion and Outlook</b>	<b>36</b>
	<b>References</b>	<b>40</b>



# 1 Introduction

The Standard Model of particle physics (SM) describes all known fundamental particles and their interactions and stands up to rigorous testing [1]. However, the nature of dark matter (DM) [2] and the origin of gravity [3], among other open questions, cannot be explained by the SM alone. Some dark matter models predict that the coupling between SM and DM particles runs via a Higgs portal. This means that the Higgs boson would decay into weakly interacting particles [4]. These are not detectable and are therefore referred to as invisible in this thesis.

There is one invisible decay of the Higgs boson in the SM, namely  $H \rightarrow ZZ \rightarrow 4\nu$ . As the branching fraction is only 0.1% of all decay channels, its detection is beyond the sensitivity of the LHC detectors and is therefore neglected in this thesis [5]. However, the branching fraction into invisible final states can be increased if the Higgs is allowed to decay into a pair of particles which are not included in the SM [6].

In this thesis, two different Higgs production channels, weak boson fusion (WBF) and associated  $ZH$  production, are investigated and compared. An overview of the work flow can be found in Figure 1.1. The signals and their most important backgrounds are generated with Monte Carlo simulations. A 100% branching ratio into stable or long-lived particles is assumed, which is a good approximation because it is in principle equivalent to invisible decays [7]. In the end, the result can easily get scaled down to the minimum branching ratio that can be detected at the 13 TeV LHC.

After event generation, the simulated samples get passed through a detector simulation. Its effects on the event samples are also investigated. The efficiencies of both channels are evaluated with a cut-and-count approach. In addition, the evaluation will also be performed with a boosted decision tree

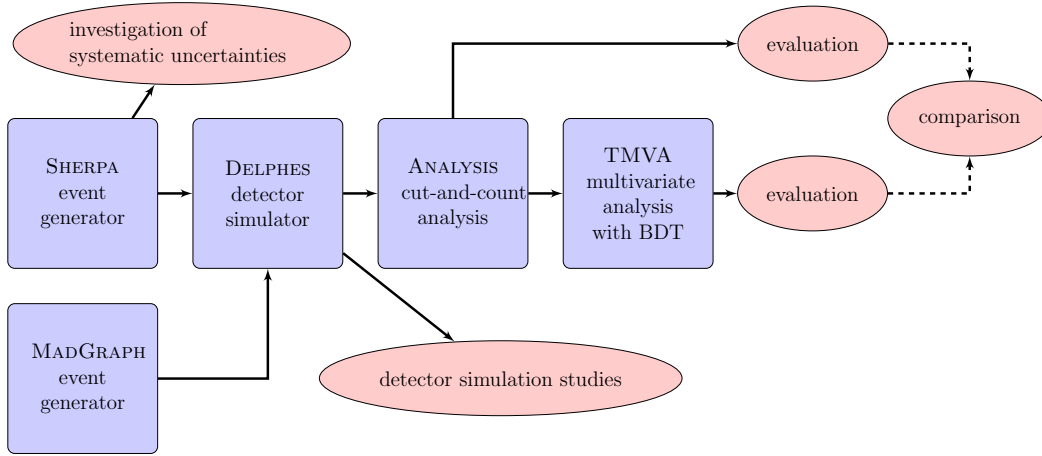


**Figure 1.1:** Work flow of this thesis. The boxes represent the software packages used, the circles the data processing.

(BDT). The importance of BDTs and other machine-learning tools has greatly increased in high energy physics during the last decade, both in theory and experiment. The performance of cut-and-count approach and the BDT are subsequently compared.

The goal of this work is to compare the WBF and the  $ZH$  production channels regarding their sensitivity to searches for invisible Higgs decays. Chapter 2 focusses on basic elements of collider physics and phenomenology, which will be important in this thesis.

Chapter 3 deals with the signals and backgrounds of the two production channels. It also describes how various software packages are used for the implementation.

In Chapter 4, the results in the WBF production channel are evaluated and in Chapter 5, the results of the associated  $ZH$  production are similarly studied. In the last chapter the results are summarized and the sensitivity of both channels to invisible Higgs decays are compared.

## 2 Phenomenology

Roughly speaking, phenomenology in particle physics makes predictions for experimental results or interprets experimental results in the framework of a theory. Monte Carlo generators are the standard tools to make predictions for SM or new physics processes which can be tested at colliders. This chapter will first outline the Standard Model and its limitations. Then various observables peculiar to high energy physics and some effects of detectors will be expounded.

### 2.1 Standard Model

	Generations of matter (fermions)			gauge bosons	scalar bosons
	I	II	III		
quarks	up $u$	charm $c$	top $t$	gluon $g$	Higgs $H$
	down $d$	strange $s$	bottom $b$	photon $\gamma$	
leptons	electron $e^-$	muon $\mu^-$	tau $\tau^-$	$Z$ boson	
	electron neutrino $\nu_e$	muon neutrino $\nu_\mu$	tau neutrino $\nu_\tau$	$W^\pm$ boson	

**Table 2.1:** Particles of the SM. This table has been created based upon [8].

The Standard Model is a theory of quantum electrodynamics, the weak theory and quantum chromodynamics and describes all known elementary particles. Table 2.1 provides an overview over all particles in the SM. It contains quarks, leptons, gauge bosons and the Higgs boson [8, 9]. Quarks and leptons are divided into three generations. The higher the generation,

the larger the mass and the shorter the lifetime is. The gauge bosons are the force carriers. Specifically, the photon  $\gamma$  carries the electromagnetic force, the  $W^\pm$  and  $Z$  bosons the weak interaction, and eight gluons  $g$  carry the strong interaction between colored particles [10, 11]. The Higgs field generates the masses of the  $W$  and  $Z$  bosons and the fermions by spontaneous symmetry breaking [12].

Even though many predictions of the SM have been measured with astonishing accuracy, some observations are unexplained, for instance the existence of dark matter [13] and the recently observed  $B$  meson anomalies [14]. These indicate that there must be new physics beyond the SM.

## 2.2 Collider Physics

In the following, commonly used observables in collider physics are introduced. These can be found, for example, in [15, 16]. Figure 2.1 provides an overview over the geometry inside a collider.

- **Transverse Momentum,  $p_T$ .** Consider a particle emitted from a collision. Then  $p_T$  is the momentum perpendicular to the beam axis,  $z$ . If the  $xy$ -plane is the plane that is orthogonal to the  $z$ -axis, the transverse momentum is calculated by

$$p_T = \sqrt{p_x^2 + p_y^2}. \quad (2.1)$$

- **Pseudorapidity,  $\eta$ .** The pseudorapidity is derived from the rapidity  $y$ , defined as

$$y = \frac{1}{2} \ln \left( \frac{E + p_z}{E - p_z} \right). \quad (2.2)$$

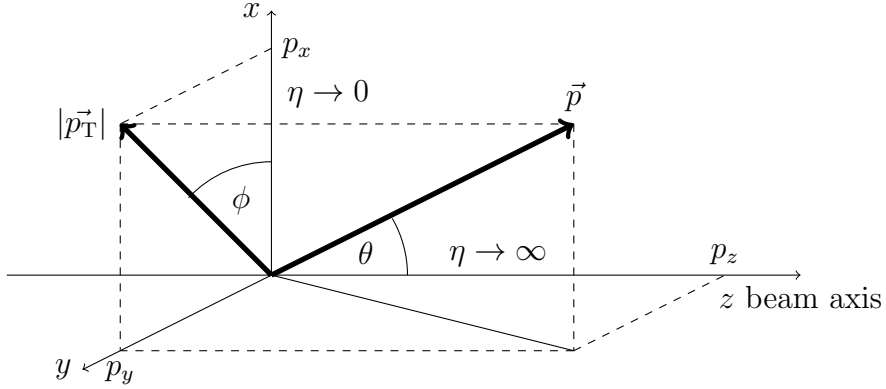


**Figure 2.1:** Schematic overview of collider geometry. The depicted observables are  $p_T$ ,  $\theta$  and  $\phi$  in a cartesian coordinate system. The particle with momentum  $\vec{p}$  is produced at the origin.

Here  $E$  is the total energy of the particle and  $p_z$  is momentum in beam direction. Then  $\eta$  is defined as  $y$  in the limit of massless particles,

$$\eta = \lim_{m \rightarrow 0} y = \lim_{m \rightarrow 0} \frac{1}{2} \ln \left( \frac{E + p_z}{E - p_z} \right) = \operatorname{artanh} \frac{p_z}{|\vec{p}|} = -\ln \tan \frac{\theta}{2}. \quad (2.3)$$

Here,  $\theta$  is the angle between the momentum  $\vec{p}$  and the positive beam direction. So,  $\eta = 0$  if  $\theta = \pi/2$  and  $\eta \rightarrow \infty$  if  $\theta \rightarrow 0$ . Even though usually massive particles are described, the usage of  $\eta$  is justified as their mass is small compared to the collider energy.

- **Azimuthal Angle,  $\phi$ .** This is the angle in the plane perpendicular to the beam direction. For symmetry reasons, the differential cross section  $d\sigma/d\phi$  is always expected to be evenly distributed from  $-\pi$  to  $\pi$ . However, the difference  $\Delta\phi$  between two particles can be a more interesting observable.

- **Distance,  $\Delta R$ .** The distance measure  $\Delta R$  between two particles is, amongst others, used in jet reconstruction. It is defined by the angular coordinates  $\eta$  and  $\phi$  as

$$\Delta R = \sqrt{(\Delta\eta)^2 + (\Delta\phi)^2}. \quad (2.4)$$

- **Invariant Mass,  $m_{AB}$ .** The invariant mass of two particles A and B is defined by their four-momenta  $P_A$  and  $P_B$  as

$$m_{AB}^2 = (P_A + P_B)^2 = m_A^2 + m_B^2 + 2E_A E_B - 2\vec{p}_A \cdot \vec{p}_B. \quad (2.5)$$

This is Lorentz-invariant by construction.

- **Missing Energy  $E^{\text{miss}}$ .** This observable should really be called missing momentum, but is usually referred to as missing energy. It is calculated by vectorially adding the three-momenta of all final particles. Specifically, as there is zero energy perpendicular to the beam direction before a collision, any net momentum afterwards indicates the existence of missing transverse energy  $E_T^{\text{miss}}$ . In the SM, missing energy arises from neutrinos but it can also come from detector effects. If an experiment finds more missing energy than predicted by SM phenomenology, this is an indication for unknown invisible particles.

A detector usually aims to measure all these properties in case of a collision. From this data, jets and particles are reconstructed. A jet is a localized peak of hadron energy interpreted as originating from a quark or gluon with the corresponding energy and direction [15, 16]. However, a perfect reconstruction of events is not possible as several sources of detector effects need to be taken into account, including smearing and failed jet reconstructions. Smearing arises because of the finite resolution of a detector.

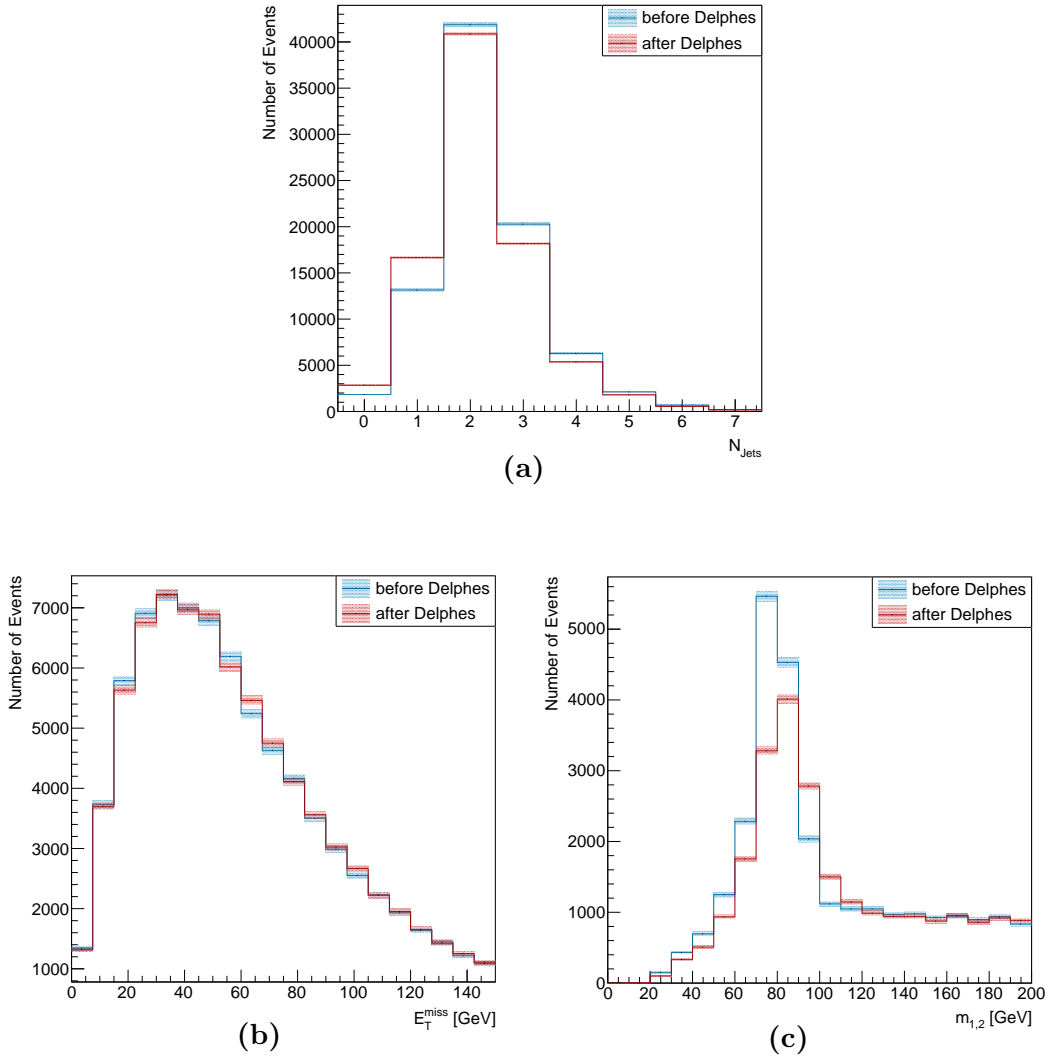


**Figure 2.2:** Distributions of the electroweak  $Z$  production,  $qq \rightarrow qqZ$ , before and after DELPHES. 2.2a: failed jet reconstruction or misidentification, 2.2b: slightly increased missing transverse energy, 2.2c: smearing in the distribution of the invariant mass of the two hardest jets. Even though the effect in the missing energy distribution is not statistically significant, it does show a tendency. All distributions include statistical errors. The events before DELPHES were processed with MADANALYSIS5 [20].

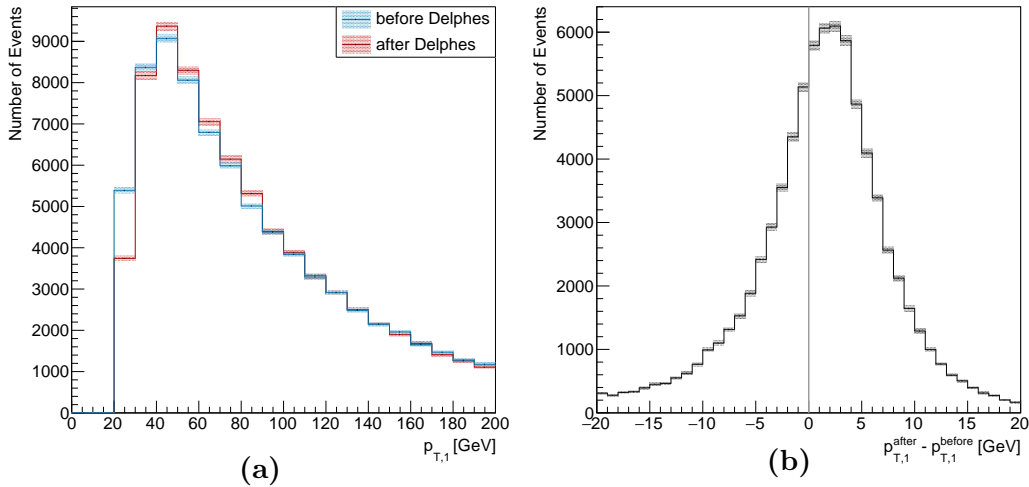


**Figure 2.3:** Distributions of the electroweak  $Z$  production,  $qq \rightarrow qqZ$ , before and after DELPHES. 2.3a: Transverse momentum of the hardest jet. 2.3b: Difference of the transverse momentum of the hardest jet. The distributions include statistical errors. The events before DELPHES were processed with MADANALYSIS5 [20]. A line at  $p_T = 0$  is included to make the shift to higher values more noticeable.

It is most prominently seen in momentum distributions, especially when kinematic cuts are applied. Failed reconstructions can arise from the finite resolution or from imperfect algorithms in the detector software. This can lead to misinterpretation of results, for instance if a three-lepton event was interpreted as a two-lepton event because one lepton got lost.

Detector effects need to be taken into account in phenomenology. To mimic these, the detector simulation DELPHES [17] is used, which includes a track propagation system with a magnetic field, electromagnetic and hadron calorimeters, and a muon identification system. Examples of detector effects can be seen in Figure 2.2. It shows results for 10,000 events of the electroweak background of the WBF channel with  $Z$  bosons. The process will be explained in more detail in Chapter 4. The hard process was generated

with MADGRAPH5 [18] and subsequently showered with PYTHIA6 [19]. All histograms are normalized to one and the distributions before and after DELPHES are compared. From the top figure one can see that the number of jets decreases after DELPHES. One can also see that  $E_T^{\text{miss}}$  slightly increases, which is expected as some particles will escape without being detected. In the distribution of the invariant mass of the two hardest jets the smearing is clearly visible.

In Figure 2.3 one can see that the transverse momentum of the hardest jet increases after DELPHES, which is rather counter-intuitive. The reason is that DELPHES takes into account that some jet energy gets lost in the detector. To compensate for that, the measured momentum gets multiplied by a jet energy scale, which is  $p_T$  and  $\eta$  dependent. This scale is greater or equal to 1, causing the distribution in Figure 2.3 to shift in the positive direction.

All these effects need to be kept in mind when analyzing the distributions and data yields in the subsequent chapters.

## 3 Production Channels

The most important production channels of the Higgs boson are gluon fusion, weak boson fusion, associated production with vector bosons and associated production with top quarks [6, 16]. Gluon fusion is not a suitable channel for the search for invisible decays. The reason is that there are no leptons, jets or other decay products at leading order, meaning that it cannot be detected. The associated Higgs production with top quarks would be a possible channel but has the disadvantage that it is harder to distinguish from the background. That is why this thesis focusses only on weak boson fusion and Higgs production in association with a  $Z$  boson.

### 3.1 Weak Boson Fusion

In weak boson fusion, a Higgs boson is created in the annihilation of two  $W^\pm$  or  $Z$  bosons. The signature of the signal is two jets with a large separation in pseudorapidity and large missing transverse momentum [22]. This ensures a good discrimination from the backgrounds. The four most important backgrounds are strongly (QCD) and weakly (EW) produced  $Z$  and  $W^\pm$ +jets processes. Example Feynman diagrams of the signal and the backgrounds are presented in Figure 3.1.

For the backgrounds, only the  $Z$  decays into neutrinos and the  $W$  decays into a lepton-neutrino pair are considered, where the lepton is not detected in case of the  $W$  decay. Other decay channels, e.g. into quark pairs, do exist and are in fact more likely than those considered here [23]. However, these do not contribute to the missing energy.

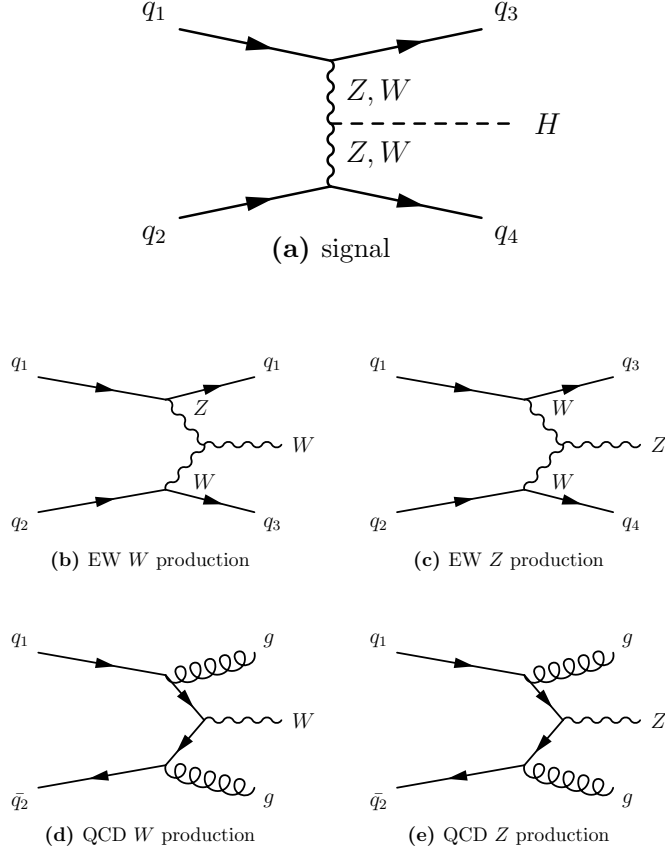


**Figure 3.1:** Example Feynman diagrams for the WBF signal and the most important backgrounds. The Higgs decays to invisible particles, the  $W$  boson to a neutrino and a misidentified lepton, and the  $Z$  boson to a neutrino pair. All Feynman diagrams have been created using FEYNMF [21].

At generator level, some cuts were used to avoid divergences and provide better efficiencies in the cut flow, which is applied after that. These are shown in Table 3.1. The cuts are chosen to be less strict than the values in the cut flow to ensure that losing events that could indeed contribute to a possible background is unlikely.

Observable	Requirement
Number of Jets	$\geq 2$
Jet diameter $\Delta R$	$< 0.4$
$p_{T,1}, p_{T,2}$	$> 20$ GeV
$ \Delta\eta_{1,2} $	$> 3$
$ \Delta\phi_{1,2} $	$< 1.3$
$m_{\text{lepton,neutrino}}$	$> 10$ GeV

**Table 3.1:** Cuts at generator level on the WBF signal and all important backgrounds. Observables denoted with  $i$  refer to the  $i$ -th hardest jet, respectively. The last requirement applies to the  $W$  production channels only.

Observable	Requirement
Number of Leptons	$= 0$
Number of Jets	$\geq 2$
$p_{T,1}, p_{T,2}$	$> 40$ GeV
$ \Delta\eta_{1,2} $	$> 4.4$
$\eta_1 \cdot \eta_2$	$< 0$
$E_T^{\text{miss}}$	$> 100$ GeV
$m_{1,2}$	$> 1.2$ TeV
$\eta_j \notin (\eta_{\min}, \eta_{\max})$ if $p_{T,j}$	$> 20$ GeV
$ \Delta\phi_{1,2} $	$< 1$

**Table 3.2:** Cut flow for the WBF signal and backgrounds. Observables denoted with  $i$  refer to the  $i$ -th hardest jet, respectively. In the seventh line,  $j > 2$  and  $\eta_{\min} = \min(\eta_1, \eta_2)$ ,  $\eta_{\max} = \max(\eta_1, \eta_2)$ .

After the generation and detector simulation, a cut flow is used to separate the signal from the backgrounds, which applies stricter cuts with each step and counts the number of events that passed after each cut. It is summarized in Table 3.2 and closely follows those suggested in [22, 24, 25]. This cut flow is not entirely state-of-the-art any more as it has been first suggested by [7] and has hardly been changed since. A lepton veto is applied to suppress the  $W$  production channels. To focus on the WBF process, the two leading jets are supposed to have a large separation in pseudorapidity and point in opposite hemispheres. Events will also be rejected if the pseudorapidity of a third jet with  $p_T > 20$  GeV is between the two leading jets. The reason why these are not wanted is linked to the color structure as virtual gluon exchange is practically absent in WBF [6]. This cut is called Central Jet Veto (CJV). The cut on the azimuthal opening angle,  $\Delta\phi$ , further suppresses multi-jet backgrounds.

## 3.2 Associated $ZH$ Production

The  $ZH$  signal is a very suitable channel for the search for invisible Higgs decays if only  $Z \rightarrow l^+l^-$  decays are considered. The  $Z \rightarrow \nu\bar{\nu}$  decay is practically impossible to detect as there is no signature. The fact that the two leptons come from the same particle makes the search much easier than in the associated  $W$  production, in which the background is very difficult to suppress [26]. Therefore, only the associated  $Z$  production is considered in this thesis. Example Feynman diagrams of the signal and the most important backgrounds are shown in Fig. 3.2. The depicted background processes are described in more detail below, ordered by decreasing importance.

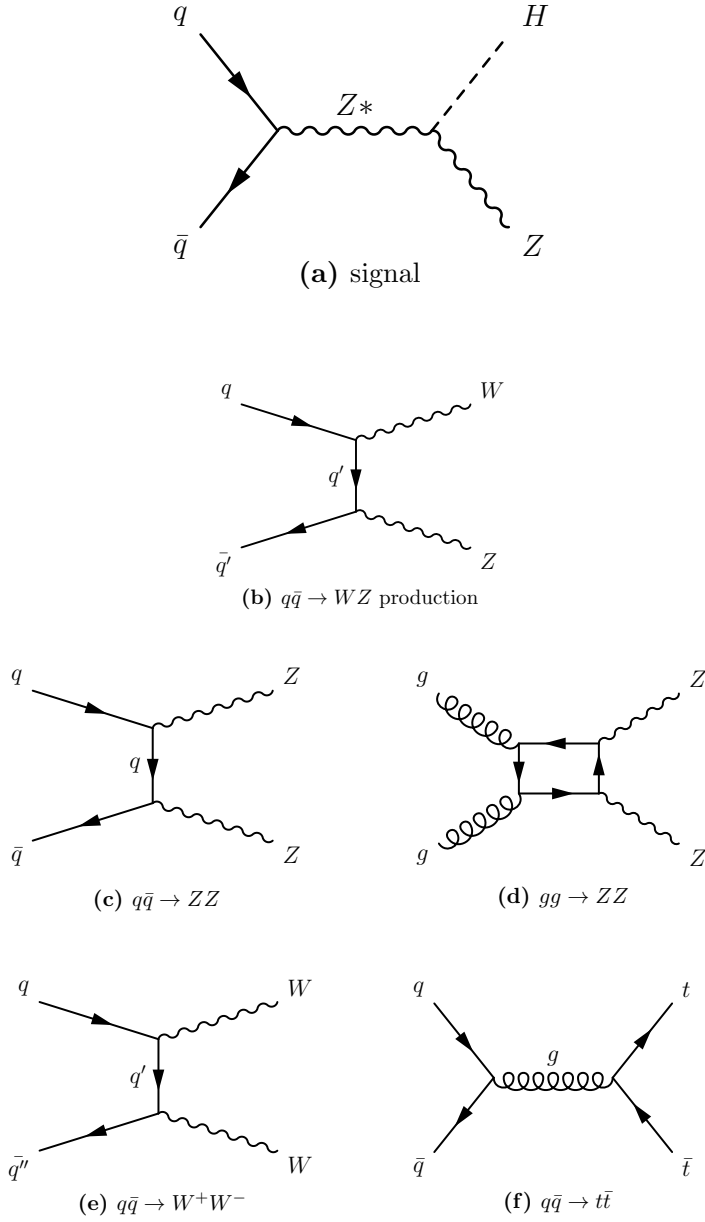


**Figure 3.2:** Example Feynman diagrams for the ZH signal and the most important backgrounds. The Higgs boson decays to invisible particles, the  $W$  boson to a neutrino and a misidentified lepton, the  $Z$  boson to a neutrino pair and the  $t$  to a  $b$  quark and a  $W$  boson.

- $q\bar{q} \rightarrow WZ$ . The  $Z$  boson is required to decay to neutrinos and the  $W$  to a lepton-neutrino-pair, where the lepton from the  $W$  decay gets lost.
- $q\bar{q} \rightarrow ZZ$ . Here one  $Z$  boson is required to decay to neutrinos and the other to leptons to match the signature of the signal.
- $gg \rightarrow ZZ$ . Even though this is a loop process, the contribution to the total background cannot be ignored.
- $q\bar{q} \rightarrow W^+W^-$ . The two leptons from the  $W$  decay have a chance of complying with the signal signature, making this process a possible background.
- $q\bar{q} \rightarrow t\bar{t}$ . The top quark mostly decays to a bottom quark and a  $W$  boson, so the above applies again.

The  $W^+W^-$  and the  $t\bar{t}$  production channels are very small and are therefore not further analyzed. Other background contributions have been found to be negligible [27, 28]. On generator level, some cuts were applied to the  $q\bar{q} \rightarrow WZ$  and  $gg \rightarrow ZZ$  backgrounds. These are shown in Table 3.3. No cuts on generator level were applied on the signal and the  $q\bar{q} \rightarrow ZZ$  production channel.

Observable	Requirement
$ m_{1,2} - m_Z $	$< 20$ GeV
$\Delta R_{1,2}$	$< 2.4$
$p_T^{1,2}$	$> 75$ GeV
$p_{T,1}, p_{T,2}$	$> 15$ GeV

**Table 3.3:** Cuts at generator level on the ZH signal and the  $q\bar{q} \rightarrow WZ$  and  $gg \rightarrow ZZ$  backgrounds. Observables denoted with  $i$  refer to the  $i$ -th hardest lepton, respectively. The short notation  $p_T^{1,2} = p_{T,1} + p_{T,2}$  was used.

Observable	Requirement
Number of SFOS Leptons	= 2
$p_{T,1}$	> 30 GeV
$p_{T,2}$	> 20 GeV
$ m_{1,2} - m_Z $	< 15 GeV
$E_T^{\text{miss}}$	> 120 GeV
$\Delta R_{1,2}$	< 1.8
$ \Delta\phi(E_T^{\text{miss}}, p_T^{1,2}) $	> 2.7
$ p_T^{\text{miss,jet}} - p_T^{1,2} /p_T^{1,2}$	< 0.2
$ \Delta\phi(E_T^{\text{miss}}, \text{jets}) $	< 0.7
$p_T^{1,2}/m_T$	< 0.9
B-tagged Jets	veto

**Table 3.4:** Cut flow for the ZH signal and backgrounds. For the definition of  $m_T$ , see text. The subscripts  $i$  refer to the  $i$ -th hardest lepton, respectively.

Similarly to the WBF channel, a cut flow closely following the experimental analysis in [27] is applied, as presented in Table 3.4. Setting the number of leptons to two and requiring same-flavor-opposite-sign (SFOS) leptons suppresses the  $W^+W^-$  and  $t\bar{t}$  production channels especially. The cuts on  $|m_{1,2} - m_Z|$  and on  $E_T^{\text{miss}}$  ensure that the lepton pair comes from the  $Z$  boson. This especially suppresses the  $t\bar{t}$  and  $W^+W^-$  backgrounds. The cut on  $E_T^{\text{miss}}$  reduces the  $t\bar{t}$  and  $W^+W^-$  backgrounds in particular. The reason is that processes with two  $W$  bosons which decay to a lepton and a neutrino each have lower missing energy because the momenta of the neutrinos point in different directions. The cut on  $\Delta R_{1,2}$  reduces the  $t\bar{t}$ ,  $W^+W^-$  and  $ZZ$  production channels because in each of these processes the leptons are not necessarily boosted. The  $|\Delta\phi(E_T^{\text{miss}}, p_T^{1,2})|$  cut further suppresses the  $t\bar{t}$  background because the  $b$ -jets can lead to fake missing energy. The  $|\Delta\phi(E_T^{\text{miss}}, \text{jets})|$  and

the  $p_T^{1,2}/m_T$  cuts reject events with fake missing energy. The transverse mass of the event  $m_T$  is defined as

$$m_T = \sqrt{2p_T^{1,2} E_T^{\text{miss}} \left[ 1 - \cos \Delta\phi(p_T^{1,2}, E_T^{\text{miss}}) \right]}. \quad (3.1)$$

Hence, for the signal we expect  $p_T^{1,2}/m_T \simeq \frac{1}{\sqrt{2}} \simeq 0.7$ . With fake missing transverse energy, for example through detector effects,  $p_T^{1,2}/m_T$  gets larger. Finally, the veto on b-tagged jets suppresses the  $t\bar{t}$  production channel.

### 3.3 Methods and Software

The event generation and analysis of both channels is performed in four steps: First of all, events are generated with SHERPA [29]. These pass through DELPHES [17], a fast detector simulation. Then the detector output passes a cut flow implemented in C++ and ROOT [30]. This way the cut-and-count approach to distinguish between signal and background will be evaluated. The data from the detector output is also prepared for the analysis by Boosted Decision Trees (BDT). The results from the BDT will finally be compared with those from the cut flow.

SHERPA calculates the matrix elements of the hard process, generates events, merges multi-jet processes and applies parton showering and hadronization. After parton showering the final state of stable particles is obtained. Hadronization is the forming of hadrons from quarks and gluons. For the setup of SHERPA, the Numbering Scheme by the Particle Data Group was used [31].

To investigate systematic uncertainties, the cross section of the process  $q\bar{q} \rightarrow ZZ$ , a background of the associated  $ZH$  production, is calculated at a

sqrt(s) [TeV]	8 LO	8 NLO	13 LO	13 NLO
paper [32]	5.060	7.369	9.887	14.51
same settings	5.062	7.35	9.884	14.48
scheme	5.329	7.34	10.405	14.50
scales	5.120	7.15	10.475	14.25
PDF	5.610	7.31	10.878	14.48
scales + scheme	5.390	7.15	11.027	14.29
PDF + scales	5.677	7.13	11.507	14.29
PDF + scheme	5.905	7.31	11.451	14.49
all default	5.976	7.14	12.113	14.30

**Table 3.5:** Comparison of paper and SHERPA results, also examining the influence of setting various parameters to SHERPA default. The uncertainties are 0.02 or smaller for all numbers.

center-of-mass-energy  $\sqrt{s}$  of 8 and 13 TeV at leading (LO) and next-to-leading order (NLO). The settings are as chosen in [32], which are the  $G_\mu$  scheme, the  $Z$  boson mass scales and the MSTW 2008 [33] set of particle-distribution functions and are compared with the SHERPA default settings in Table 3.5.

Interestingly, setting the scheme, scales and PDF to default results in a slight decrease of the cross section at NLO of up to 3 %, but a big increase at LO of up to 23% in comparison to the settings used in [32]. Of these, about 10% are due to the PDF uncertainty. As in this thesis all simulations are carried out at leading order and the cross section at NNLO is then estimated with k-factors, an uncertainty of about 10% should always be taken into account next to the statistical uncertainties.

The SHERPA output is passed to the DELPHES ATLAS detector simulation. The cut flow of each channel, as presented in Tables 3.2 and 3.4, is implemented in a ROOT script. This script passes all previously generated events through each step of the cut flow individually and calculates the cross section after each cut. Also, the DELPHES output files are prepared for the BDT application.

The BDT are part of the Toolkit for Multivariate Analysis TMVA [34]. A BDT is a binary tree structured classifier which can distinguish signal from background events. It works in three phases: training, testing, and application. Training builds the tree by taking the original sample and applying a random cut on it, thus dividing it into two distinct groups. Then the purity of these groups is evaluated, which indicates the distinguishing power of the BDT. After that, more decisions are applied to this sample until the purity of all groups is high enough. Perfect splitting between signal and background is usually not ideal as this would make the tree very specific for the training sample and could not be applied to other samples as well. This phenomenon is called overtraining. To increase the scope of the BDT from the sample it trained on to other samples, it gets boosted, which means a lot of trees are generated by testing on the original sample with slightly modified weights. Then these trees get averaged. In the end this, this tree can be applied to a sample with unknown classification. In this thesis, the training and testing is performed and evaluated, but not the application to data.

The reason why the data gets passed through a cut flow and a BDT is to investigate the performance of multivariate analysis tools in comparison to cut-and-count analyses. All calculations have been carried out on BWUNICLUSTER [35].

# 4 Results in Weak Boson Fusion

## 4.1 Cut Flow

In Table 4.1 the expected data yields of the signal and the backgrounds after each individual cut are given. These are obtained by running a BDT with the same preselection cuts as the cut flow and with settings as specified in 4.2. The cross sections are at LO only and are taken directly from SHERPA. They are not calculated to higher orders with k-factors because the results would be distorted by the cuts that were applied at generator level.

Cut	Signal	EW $W$	EW $Z$	QCD $W$	QCD $Z$
before all	8.58e-1	5.31	1.94e-1	636.76	132.30
Lepton Veto	8.43e-1	2.37	1.91e-1	303.10	130.98
Jet Veto	6.57e-1	1.50	1.22e-1	153.46	58.61
$p_{T,1}, p_{T,2}$	4.26e-1	7.17e-1	8.48e-2	78.32	30.30
$ \Delta\eta_{1,2} $	1.03e-1	1.06e-1	1.85e-2	6.62	3.24
$ \eta_1 \cdot \eta_2 $	1.03e-1	1.06e-1	1.84e-2	6.62	3.24
$E_T^{\text{miss}}$	8.92e-2	3.59e-2	1.73e-2	2.92	2.35
$m_{1,2}$	3.04e-2	9.35e-3	8.42e-3	1.78	1.23
CJV	2.24e-2	5.42e-3	5.84e-3	6.49e-1	5.38e-1
$ \Delta\phi_{1,2} $	1.54e-2	3.08e-3	4.00e-3	4.07e-1	3.51e-1
Efficiency	1.80e-2	5.80e-4	2.06e-2	6.39e-4	2.65e-3

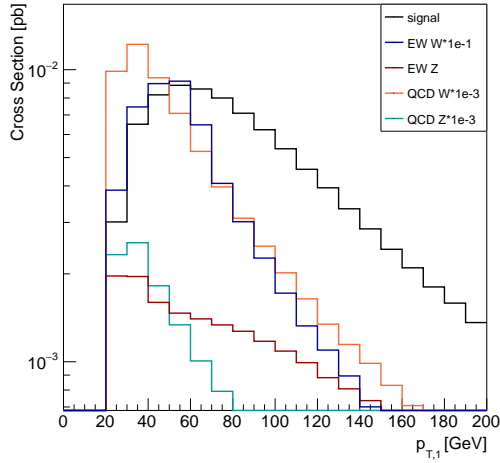
**Table 4.1:** Signal expectations and background contributions after each step of the cut flow. All cross sections are given in units of pb. The statistical uncertainties on the cross sections are: signal 0.1%, EW  $W$  0.3%, EW  $Z$  0.3%, QCD  $W$  0.3%, QCD  $Z$  2.3%. The systematic uncertainties of Monte Carlo-based predictions amounts to about 10% from particle distribution functions and the luminosity uncertainty, as found in Section 3.3. All data is generated with SHERPA at LO.

Figure 4.1 depicts various distributions of the WBF signal and its most important backgrounds before all cuts. The distributions are presented without statistical errors as these are rather small in this case, considering the sample sizes of 10 million events for the QCD  $W$  channel and 1 million events for all other channels.

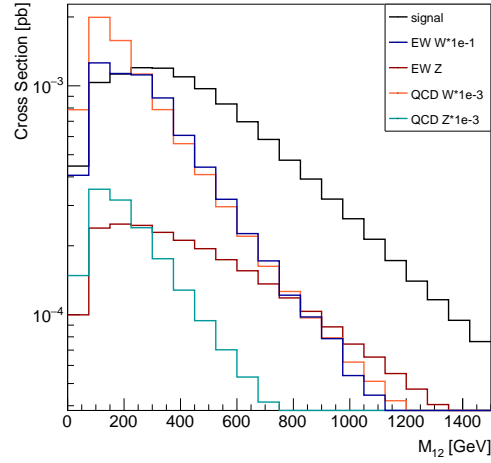
Figure 4.1a illustrates why the cut on  $p_{T,1}$  and  $p_{T,2}$  are so effective. Compared to the backgrounds, the signal has very hard leading jets. One can also see from the  $p_T$  distribution that the QCD processes would diverge when  $p_T \rightarrow 0$ . In contrast, the  $p_{T,1}$  of the EW processes and the signal decrease at lower values. This is the soft divergence in QCD processes which is cut out at generator level.

The cut on the invariant mass is justified by the distribution in Figure 4.1b. As the invariant mass is closely connected to the energy of the two hardest jets, as can be seen in equation 2.5, the soft divergence is clearly to be seen in the distributions of the QCD processes. If the available amount of data is big enough, one could make the cut on  $m_{1,2}$  even stricter, thus increasing the signal-to-background ratio.

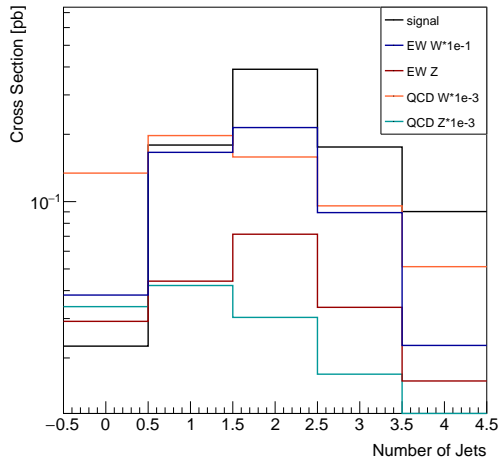
From the distributions of the number of jets (Figure 4.1c) and the number of leptons (Figure 4.1d), one can clearly see that the backgrounds are best suppressed at the cut values specified in Table 3.2. The cut on the number of jets suppresses the QCD processes especially, not only because they have a large cross section to begin with, but also because the distributions reach their maxima at  $N_{\text{jets}} = 1$  and are still sizeable at  $N_{\text{jets}} = 0$ . The cut on the leptons also increases the signal-to-background ratio as the signal is highest at zero leptons, but especially the  $W$  production channels are not. The reason why a signal event can have more than zero leptons is that some leptons occur in jets.



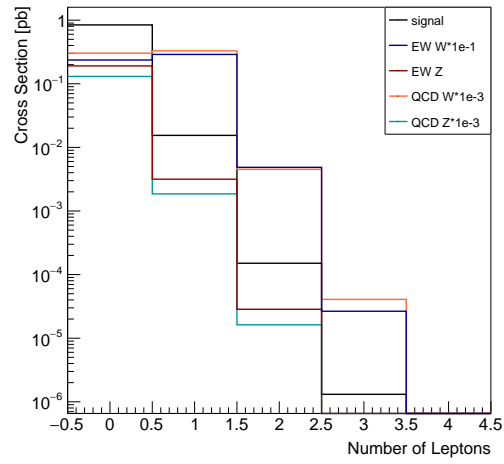
(a)  $p_T$  of hardest jet.



(b) Invariant mass of two hardest jets.



(c) Number of jets.



(d) Number of leptons.

**Figure 4.1:** Distributions before all cuts. Some samples have been scaled for better visibility as can be seen in the legends.

## 4.2 Boosted Decision Trees

In this section, the performance of the BDT in comparison to the cut-and-count approach is investigated. Also, the performance of BDTs with simple variables and more sophisticated ones are compared. All BDTs consist of 400 trees with three layers and have been checked against overtraining. The variables used in the tree are

$$p_{T,1}, \eta_1, \phi_1, p_{T,2}, \eta_2, \phi_2, E_T^{\text{miss}}, \phi_{E_T^{\text{miss}}}, m_{1,2}. \quad (4.1)$$

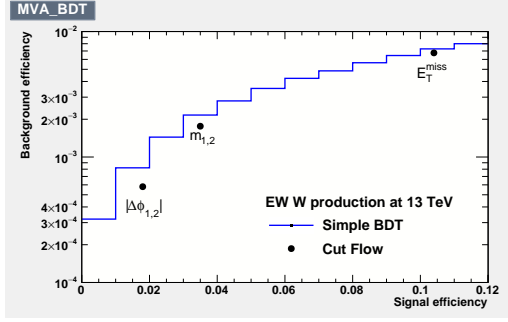
These are basic variables which require no deeper understanding of the involved processes. In addition to those mentioned above, the variables used in the more sophisticated tree are

$$|\Delta\eta_{1,2}|, |\Delta\phi_{1,2}|, N_{\text{leptons}}, N_{\text{jets}}. \quad (4.2)$$

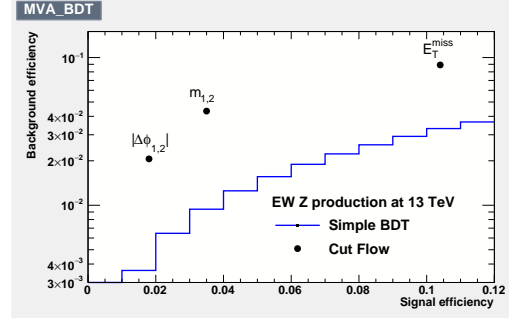
The choice for these variables is motivated by those in the cut-and-count approach.

In Figure 4.2, the receiver operating characteristics curves (ROC curves), which are the background efficiencies as a function of the signal efficiency, can be seen of the most important backgrounds against the signal.

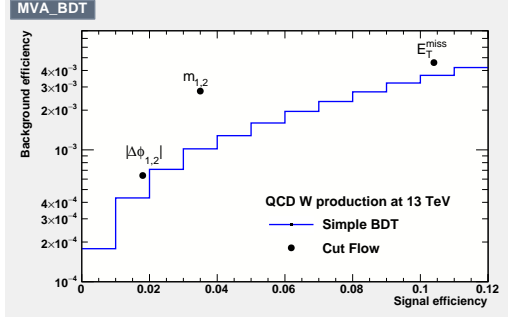
The BDT of the EW  $W$  production in Figure 4.2a performs slightly worse than the cut flow. At the same signal efficiency, the BDT increases the background efficiency by about 42% in comparison to the cut flow after all cuts. However, this is not very much given that the background efficiency and the data yield after all cuts are rather low compared to the signal, as can be seen in Table 4.1.



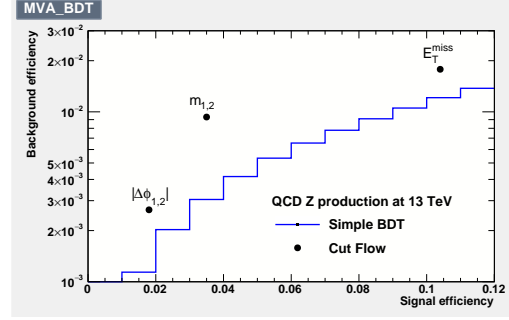
(a) EW  $W$  production. Rank of variables in BDT:  $E_T^{\text{miss}}$ ,  $p_{T,1}$ ,  $m_{1,2}$ ,  $p_{T,2}$ ,  $\eta_2$ ,  $\phi_2$ ,  $\eta_1$ ,  $\phi_1$ ,  $\phi_{E_T^{\text{miss}}}$ .



(b) EW  $Z$  production. Rank of variables in BDT:  $E_T^{\text{miss}}$ ,  $p_{T,1}$ ,  $\eta_1$ ,  $\phi_1$ ,  $p_{T,2}$ ,  $m_{1,2}$ ,  $\eta_2$ ,  $\phi_2$ ,  $\phi_{E_T^{\text{miss}}}$ .



(c) QCD  $W$  production. Rank of variables in BDT:  $E_T^{\text{miss}}$ ,  $\eta_1$ ,  $p_{T,1}$ ,  $\eta_2$ ,  $m_{1,2}$ ,  $\phi_1$ ,  $\phi_{E_T^{\text{miss}}}$ ,  $p_{T,2}$ ,  $\phi_2$ .



(d) QCD  $Z$  production. Rank of variables in BDT:  $E_T^{\text{miss}}$ ,  $\eta_1$ ,  $m_{1,2}$ ,  $\eta_2$ ,  $p_{T,1}$ ,  $p_{T,2}$ ,  $\phi_2$ ,  $\phi_1$ ,  $\phi_{E_T^{\text{miss}}}$ .

**Figure 4.2:** ROC curves of the most important backgrounds against the WBF signal. The black dots refer to the efficiencies of the cut flow after the cut on the observable specified on the label.

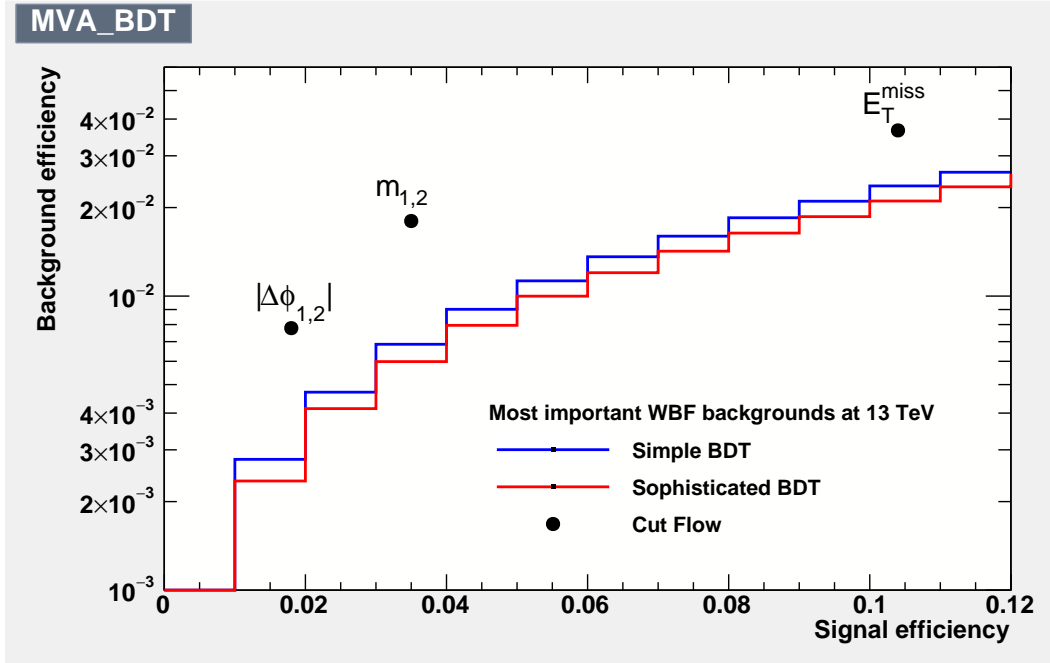


**Figure 4.3:** Simple and sophisticated ROC curves of all backgrounds against the WBF signal. The black dots refer to the efficiencies of the cut flow after the cut on the observable specified on the label. Rank of variables in BDT (observables in brackets apply to the sophisticated BDT only):  $E_T^{\text{miss}}$ ,  $p_{T,1}$ , ( $N_{\text{jets}}$ ),  $m_{1,2}$ , ( $|\Delta\eta_{1,2}|$ ), ( $N_{\text{leptons}}$ ), ( $|\Delta\phi_{1,2}|$ ),  $\eta_1$ ,  $p_{T,2}$ ,  $\phi_1$ ,  $\eta_2$ ,  $\phi_2$ ,  $\eta_{E_T^{\text{miss}}}$ ,  $\phi_{E_T^{\text{miss}}}$ .

The BDT of the EW  $Z$  production, to be seen in Figure 4.2b, decreases the background efficiency by about 81%. This is a lot, considering that this background is very similar to the signal and therefore irreducible with the cut-and-count approach. As can be seen in Table 4.1, in the cut flow the efficiency of the EW  $Z$  channel is actually higher than that of the signal. A possible reason for this great decrease is that this channel could be better suppressed with a stricter cut on  $p_{T,1}$ ,  $p_{T,2}$  and  $E_T^{\text{miss}}$ . Also, a cut on  $\phi_1$  could be applied after a cut on  $\eta_1$  (and for  $\phi_2$  and  $\eta_2$  analogously). An indication that it was done can be found in the rank of the variables in the BDT of the EW  $Z$  production channel.

In the QCD  $W$  production in Figure 4.2c, the BDT reduces the background efficiency by approximately 31% at the same signal efficiency. This is a large amount as this channel contributes 53% to the total background.

The BDT reduces the background of the QCD  $Z$  production by about 53%, which is a similarly large amount as that of the QCD  $W$  production. It contributes about 46% to the total background. The ROC curve can be seen in Figure 4.2d.

Figure 4.3 shows the ROC curves of a simple BDT with the simple variables of Equation 4.1 and a more sophisticated BDT with the variables of Equations 4.1 and 4.2. The more sophisticated BDT performs a little better than the simple one. However, the difference between the simple and the sophisticated tree less than 10% throughout the depicted range. After all cuts, the simple BDT decreases the total background efficiency by about 68% at same signal efficiency, the more sophisticated one by 69%.

All in all, in the WBF production channel the usage of a BDT can increase the signal-to-background ratio to more than three times the ratio after the cut-and-count approach. Using more sophisticated variables in the BDT does not have a large influence on the overall performance.

# 5 Results in Associated $ZH$ Production

## 5.1 Cut Flow

In Table 5.1 the expected data yields of the signal and the most important backgrounds at QCD NNLO and EW NLO after each individual cut are given, analogously to Chapter 4. The data yields for the  $q\bar{q} \rightarrow W^+W^-$  and  $q\bar{q} \rightarrow t\bar{t}$  production channels are not shown because they are very small and statistically insignificant with the generated amount of events. The events were generated

Cut	Signal	$q\bar{q} \rightarrow WZ$	$q\bar{q} \rightarrow ZZ$	$gg \rightarrow ZZ$
before all	5.95e-2	7.33e-1	1.03	1.79e-1
SFOS Leptons	2.78e-2	1.03e-1	1.62e-1	7.21e-2
$p_{T,1}, p_{T,2}$	2.40e-2	7.29e-2	1.37e-1	6.12e-2
$ m_{1,2} - m_Z $	2.30e-2	5.25e-2	1.30e-1	4.46e-2
$E_T^{\text{miss}}$	6.07e-3	1.24e-2	1.10e-2	1.67e-3
$\Delta R_{1,2}$	5.60e-3	1.05e-2	9.21e-3	1.06e-3
$ \Delta\phi(E_T^{\text{miss}}, p_T^{1,2}) $	2.56e-3	4.74e-3	4.00e-3	4.24e-4
$ p_T^{\text{miss,jet}} - p_T^{1,2} /p_T^{1,2}$	2.50e-3	4.46e-3	3.85e-3	3.88e-4
$ \Delta\phi(E_T^{\text{miss}}, \text{jets}) $	2.30e-4	3.99e-3	4.54e-4	5.91e-5
$p_T^{1,2}/m_T$	2.30e-4	3.99e-3	4.54e-4	5.91e-5
$b$ -Jets Veto	2.20e-4	3.87e-3	4.33e-4	5.37e-5
Efficiency	3.70e-3	5.28e-4	6.50e-3	3.00e-4

**Table 5.1:** Signal expectations and background contributions after each step of the cut flow. The factor e-x means  $10^{-x}$ . All cross sections are given in units of pb. The statistical uncertainties on the cross sections are: signal 1%,  $q\bar{q} \rightarrow WZ$  5%,  $q\bar{q} \rightarrow ZZ$  0.1%,  $gg \rightarrow ZZ$  2%. The systematic uncertainties of Monte Carlo-based predictions amount to about 10% from particle distribution functions and the luminosity uncertainty, as found in Section 3.3. The last line shows the efficiencies of each channel.

with SHERPA at LO, and were scaled to the NNLO value. The cross sections were taken from [37] for the signal, from [38] for the  $q\bar{q} \rightarrow WZ$ , from [32] for the  $q\bar{q} \rightarrow ZZ$  and  $gg \rightarrow ZZ$  processes, from [39]  $q\bar{q} \rightarrow W^+W^-$ , and from [40] for  $q\bar{q} \rightarrow t\bar{t}$ , assuming that the higher-order contributions pass the cut flow the same way the LO contributions do.

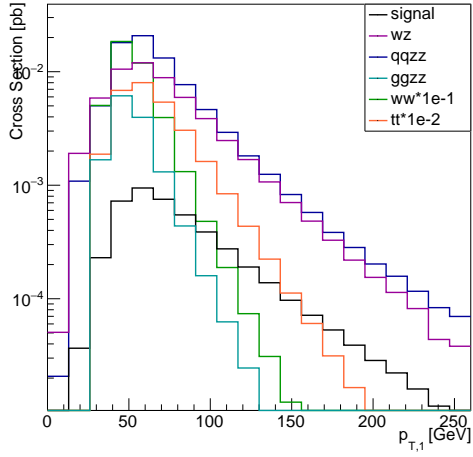
Figure 5.1 shows distributions of the ZH signal and its most important backgrounds before all cuts, including the  $W^+W^-$  and  $t\bar{t}$  processes. The distributions are presented without statistical errors as these are rather small, considering the sample sizes of 1 million events for all channels.

The distribution in Figure 5.1a implies that the cut on  $p_T$  suppresses all backgrounds similarly well. With large enough data samples, one could cut at higher values between 150 to 200 GeV in order to further suppress the  $gg \rightarrow ZZ$ , the  $W^+W^-$  and the  $t\bar{t}$  production channels.

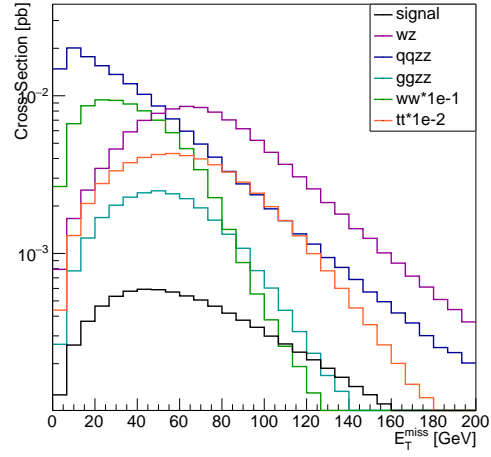
The cut on  $E_T^{\text{miss}}$  effectively suppresses the  $e W^+W^-$  and the  $gg \rightarrow ZZ$  production channels, as can be seen in Figure 5.1b. Cutting at a higher value would not be reasonable as the signal efficiency would get very small and the  $WZ$  and the  $q\bar{q} \rightarrow ZZ$  production channels would hardly be suppressed.

In Figure 5.1c one can clearly see that the signal, the  $q\bar{q} \rightarrow WZ$  and  $q\bar{q} \rightarrow ZZ$  production channels peak at the mass of the  $Z$  boson. This is expected as the two hardest leptons must come from the  $Z$  decay. The  $W^+W^-$  and the  $t\bar{t}$  production channels have a flat  $m_{1,2}$  distribution because the leptons come from two different  $W$  bosons. As the peaks of the backgrounds around the mass of the  $Z$  boson are broader than that of the signal, the  $m_{1,2}$  cut is justified.

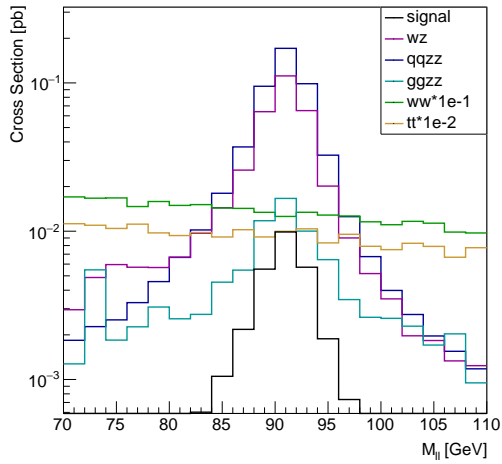
The cut on  $N_{\text{leptons}}$  mainly suppresses the  $WZ$  and  $ZZ$  production channels, as to be seen in Figure 5.1d. The requirement that the lepton pair be SFOS also reduces the  $W^+W^-$  and  $t\bar{t}$  production channels.



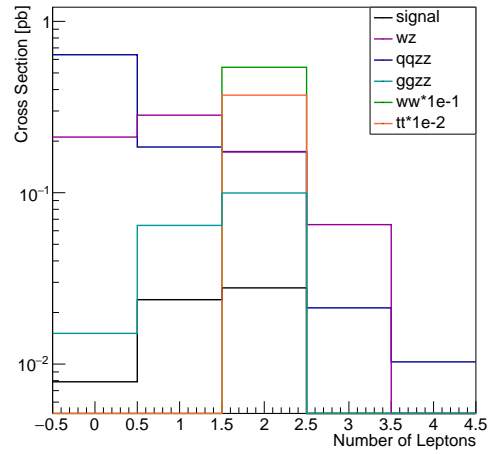
(a)  $p_T$  of hardest lepton.



(b)  $E_T^{\text{miss}}$ .



(c)  $m_{1,2}$  of the two hardest leptons.



(d)  $N_{\text{leptons}}$ .

**Figure 5.1:** Distributions before all cuts. Some distributions have been scaled down for better visibility, as can be seen in the legend.

## 5.2 Boosted Decision Trees

Similarly to Chapter 4.2, a BDT with 400 trees with three layers is used for each background individually and for all of them together. The variables used in the simple and those added in the more sophisticated BDT, respectively, are

$$p_{T,1}, \eta_1, \phi_1, p_{T,2}, \eta_2, \phi_2, E_T^{\text{miss}}, \phi_{E_T^{\text{miss}}}, m_{1,2}, \quad (5.1)$$

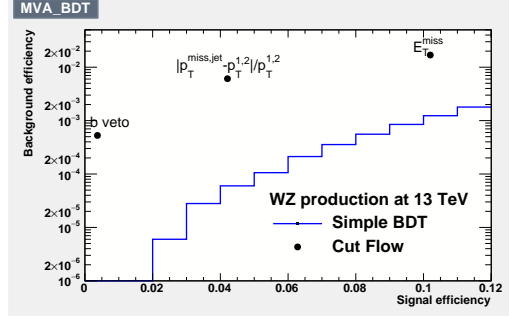
$$\begin{aligned} N_{\text{b-jets}}, N_{\text{leptons}}, |\Delta\phi_{1,2}|, |\Delta\phi(E_T^{\text{miss}}, p_T^{1,2})|, \\ |\Delta R_{1,2}|, |p_T^{\text{miss,jet}} - p_T^{1,2}|/p_T^{1,2}, p_T^{1,2}/m_T. \end{aligned} \quad (5.2)$$

Also,  $|m_{1,2} - m_Z|$  is used instead of  $m_{1,2}$ . The more sophisticated variables are motivated by the choices in the cut-and-count approach. All BDT were checked against overtraining. The ROC curves of the BDTs against the most important backgrounds are depicted in Figure 5.2.

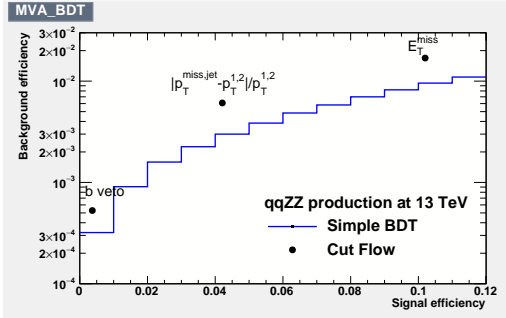
The BDT suppresses the  $WZ$  production completely at the signal efficiency of the last cut, as can be seen in Figure 5.2a. The background efficiency only gets non-zero at values above a signal efficiency of about 0.04. This is a very good performance given that the  $WZ$  production contributes about 89% to the total background, as can be seen from Table 5.1.

The BDT of the  $q\bar{q} \rightarrow ZZ$  production channel reduces the background efficiency by about 23% at the same signal efficiency after all cuts of the cut flow. The ROC curve can be seen in Figure 5.2b.

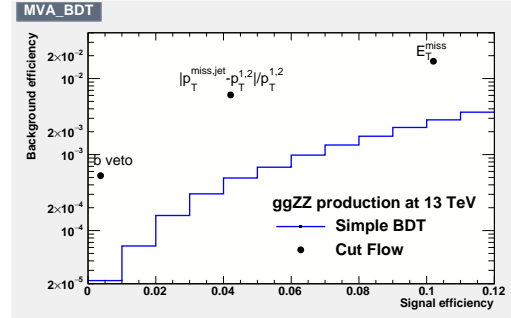
Figure 5.2c shows that the BDT reduces the background efficiency by 93% at same signal efficiency in the  $gg \rightarrow ZZ$  production channel. However, the influence on the overall BDT is rather low because the contribution of this process to the total background is rather small.



(a)  $WZ$  production. Rank of variables in BDT:  $m_{1,2}$ ,  $E_T^{\text{miss}}$ ,  $p_{T,2}, p_{T,1}$ ,  $\phi_2$ ,  $\phi_{E_T^{\text{miss}}}$ ,  $\eta_2$ ,  $\phi_1, \eta_1$ .

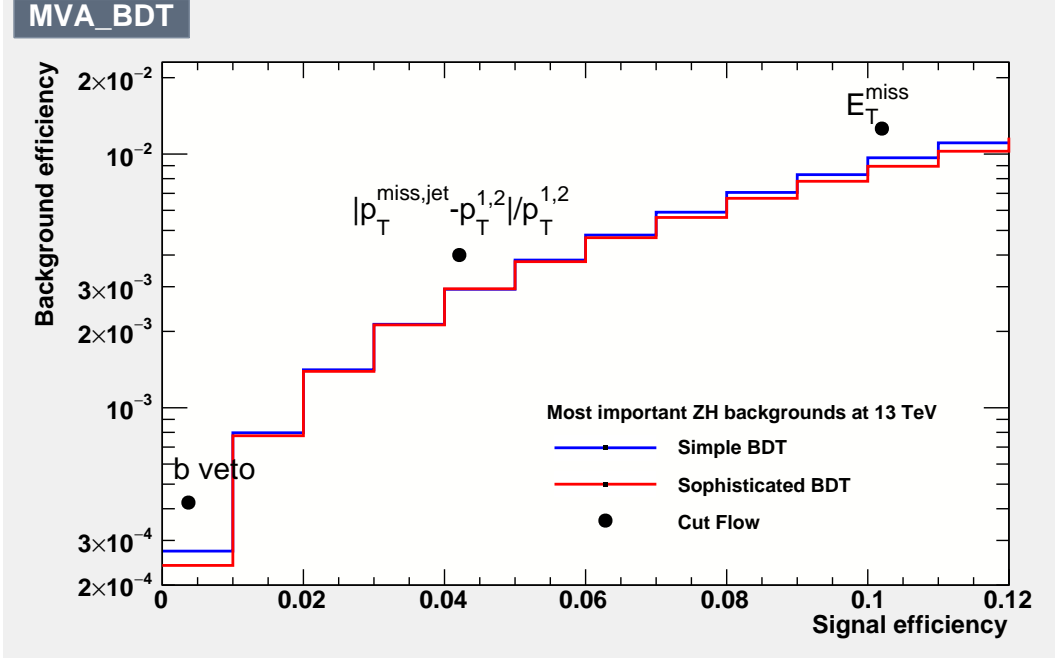


(b)  $q\bar{q} \rightarrow ZZ$  production. Rank of variables in BDT:  $E_T^{\text{miss}}$ ,  $p_{T,2}$ ,  $m_{1,2}$ ,  $\eta_1$ ,  $p_{T,1}$ ,  $\phi_1$ ,  $\phi_2$ ,  $\phi_{E_T^{\text{miss}}}$ ,  $\eta_2$ .



(c)  $gg \rightarrow ZZ$  production. Rank of variables in BDT:  $m_{1,2}$ ,  $E_T^{\text{miss}}$ ,  $p_{T,1}, p_{T,2}$ ,  $\eta_1, \eta_2$ ,  $\phi_1, \phi_{E_T^{\text{miss}}}, \phi_2$ .

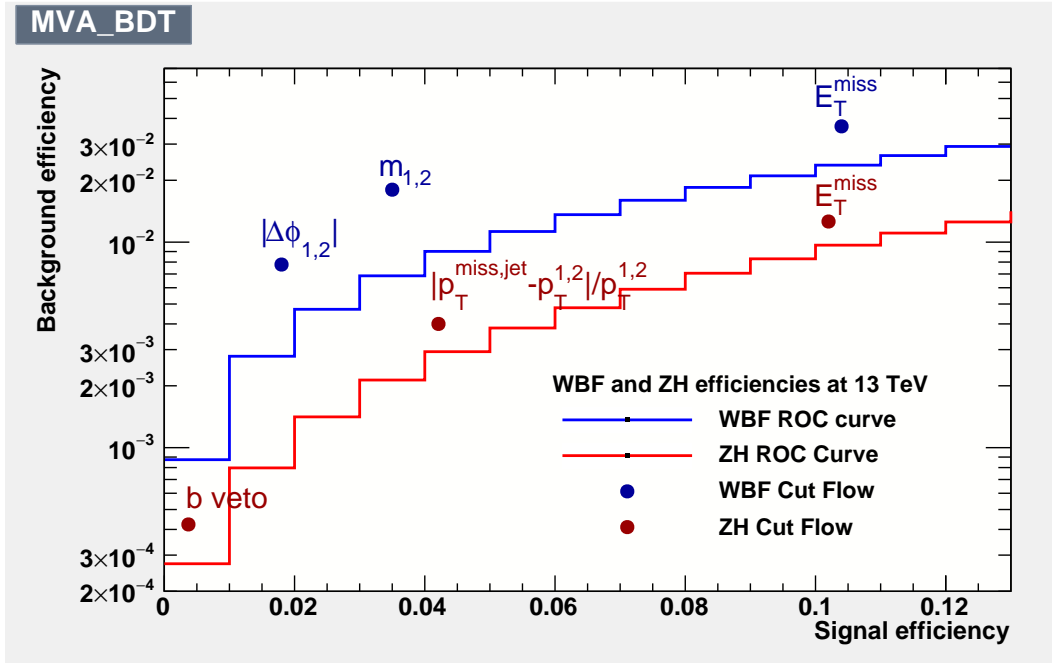
**Figure 5.2:** Simple ROC Curve of BDT of the signal against the most important backgrounds. The black dots are the results from the cut flow after the cut on the observable specified on the label.



**Figure 5.3:** ROC curves of the  $q\bar{q} \rightarrow ZZ$  and the  $q\bar{q} \rightarrow WZ$  production channels together. The black dots are the results from the cut flow after the cut on the observable specified on the label. Rank of variables in BDT (observables in brackets apply to the sophisticated BDT only):  $m_{1,2}$  (or  $|m_{1,2} - m_Z|$ ),  $(N_{\text{leptons}})$ ,  $(|\Delta\phi_{1,2}|)$ ,  $p_{T,2}$ ,  $\eta_2$ ,  $E_T^{\text{miss}}$ ,  $\eta_1$ ,  $\phi_2$ ,  $(|\Delta R_{1,2}|)$ ,  $\phi_1$ ,  $p_{T,1}$ ,  $(|p_T^{\text{miss,jet}} - p_T^{1,2}|/p_T^{1,2})$ ,  $(\Delta\phi(E_T^{\text{miss}}), p_T^{1,2})$ ,  $\phi_{E_T^{\text{miss}}}$ ,  $(p_T^{1,2}/m_T)$ ,  $(N_{\text{b-jets}})$ .

The performances of the three aforementioned BDTs suggest that stricter cuts in the cut flow could improve the search for invisible Higgs decays. Even so, the overall BDT only decreases the background efficiency by 27% with the simple variables, and by 33% with the sophisticated ones. In this production channel, the usage of a more sophisticated BDT improves the search a little more. The simple BDT increases the signal-to-background ratio by about 37%, the sophisticated one by about 49%. A possible reason why the performance of the total BDT is not overwhelmingly good is that the  $WZ$  and the  $ZZ$  production channels are very different from one another. This would make the application of effective cuts harder for the BDT.

## 6 Comparison



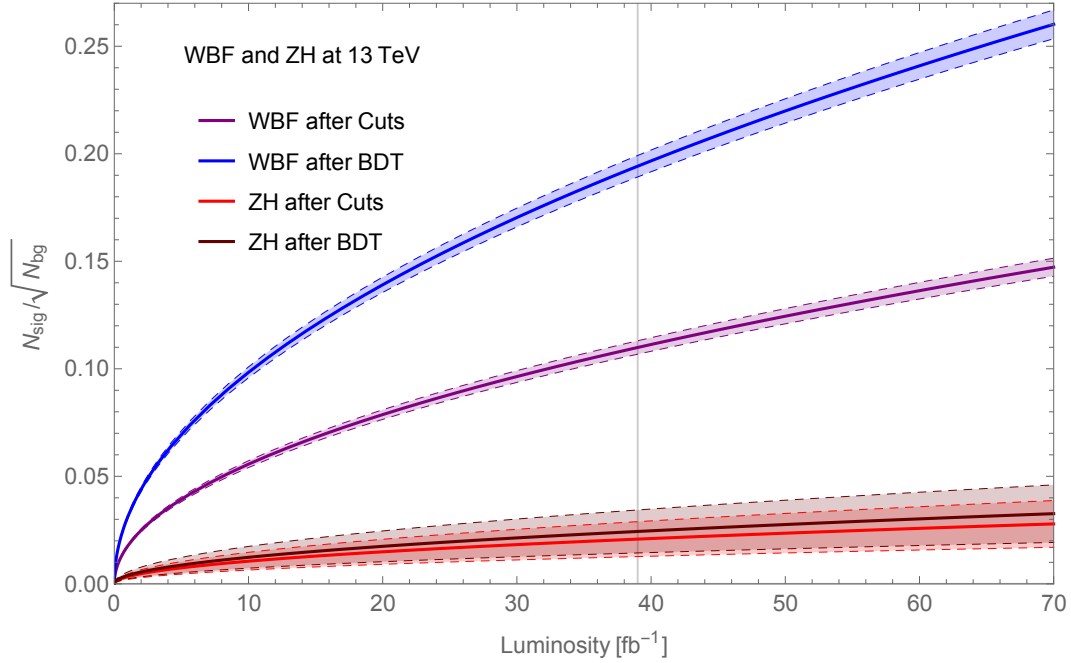
**Figure 6.1:** Comparison of the ROC curves of the simple BDTs and cut flow efficiencies of the WBF channel and the associated ZH production. The WBF ROC curve includes all mentioned backgrounds, the ZH ROC curve includes the  $WZ$  and  $ZZ$  production channels. The rank of the variables in the BDTs is as stated for the simple trees in Figures 4.3 and 5.3. The efficiencies of the WBF and ZH channel are given after the cut on the observable specified on the label.

Figure 6.1 shows the performances of the cut-and-count approach and the BDTs of both production channels. One can clearly see that the background efficiencies of the ROC curve and the cut flow of the WBF channel is about twice as large as that of the associated ZH production at same signal efficiency. On the other hand, the improvement of the simple BDT in comparison to the cut flow is 68% in the WBF channel, compared to only 27% in the associated ZH production.

As can be seen in Table 6.1, the signal-to-background ratio of the associated ZH production is about 2.5 times larger than that of the WBF channel after all cuts. As the application of the BDT especially reduces the backgrounds of the WBF channel, the ratio gets very similar to that of the associated ZH production. The performances of the simple and the more sophisticated BDTs are very similar, differing by 10% at most in the signal-to-background ratio and the significance  $S/\sqrt{B}$ . Even though the signal-to-background ratio is larger in the associated ZH production, the significance of the WBF channel is five times larger than that of the associated ZH production after the cut-to-count approach, and eight times higher after the simple BDT.

	WBF	ZH
cut-to-count approach ( $\cdot 10^{-2}$ )		
$S/B$	$2.01 \pm 0.10$	$5.05 \pm 0.37$
$S/\sqrt{B}$ [pb $^{-1/2}$ ]	$1.76 \pm 0.05$	$0.33 \pm 0.01$
simple boosted decision trees ( $\cdot 10^{-2}$ )		
$S/B$	$6.29 \pm 0.32$	$6.92 \pm 0.50$
$S/\sqrt{B}$ [pb $^{-1/2}$ ]	$3.11 \pm 0.08$	$0.39 \pm 0.02$
sophisticated boosted decision trees ( $\cdot 10^{-2}$ )		
$S/B$	$6.49 \pm 0.33$	$7.54 \pm 0.50$
$S/\sqrt{B}$ [pb $^{-1/2}$ ]	$3.16 \pm 0.09$	$0.41 \pm 0.02$

**Table 6.1:** Summary of the results of the cut-to-count approach and the BDTs at 13 TeV. The uncertainties are statistical uncertainties on the cross section and the passed events only.  $S$  refers to the cross section of the signal,  $B$  to the total cross section of the background after all cuts.



**Figure 6.2:** Comparison of WBF and ZH performances at luminosities up to  $50\text{fb}^{-1}$ . The filled areas represent the  $1\sigma$ -range of statistical uncertainties. The vertical gray line refers to the integrated luminosity at 13 TeV in 2016. This plot was generated with WOLFRAM MATHEMATICA [41].

This can also be seen in Figure 6.2, in which a plot of the ratio of the number of events  $N_{\text{sig}}/\sqrt{N_{\text{bg}}}$  after the cut flow and after the BDT is drawn as a function of the luminosity. Denoting cross sections as  $\sigma$ , this follows the equation

$$\frac{N_{\text{sig}}}{\sqrt{N_{\text{bg}}}} = \frac{\sigma_{\text{sig}} \cdot L}{\sqrt{\sigma_{\text{bg}} \cdot L}} = \frac{\sigma_{\text{sig}}}{\sqrt{\sigma_{\text{bg}}}} \cdot \sqrt{L}. \quad (6.1)$$

It is clear that the improvement from the BDT is rather small in the associated ZH production. In contrast, the significance almost doubles in WBF due to the BDT. This means that the WBF channel profits much more from a high amount of data than the ZH, especially when a BDT is used.

## 7 Conclusion and Outlook

In this thesis, the sensitivity of the WBF channel and the associated ZH production in the search for invisible Higgs decays at 13 TeV has been investigated. The cut flow of the associated ZH production could be improved by setting the cut on the missing energy from 90 GeV to 120 GeV. After the cut flow, the signal-to-background ratio of the associated ZH production is found to be about 2.5 times larger than that of the WBF channel. However, the WBF channel profits much more from large amounts of data, as  $S/\sqrt{B}$  is more than five times larger than in ZH after all cuts. So if only a cut flow is used and a relatively small amount of data is available, the associated ZH production is preferred.

Using a BDT with simple variables increases the signal-to-background ratio of the WBF channel more than three-fold. In contrast to that, the ratio increases only by about 37% in ZH, making the signal-to-background ratios of the channels very similar. As the profit of data in WBF is about 8 times as large as in ZH, the WBF channel is favoured in the search for invisible Higgs decays if BDT are used.

With more sophisticated variables the performance of the BDT is improved by a maximum of 10%. This implies that simple BDTs are sufficient to use in most cases. In future work, this knowledge can be particularly useful in the investigation of a process with an unknown signature.

The performance of other tools rather than BDTs could also be investigated. With higher energies one could also perform the search for invisible decays of a Higgs boson in other production channels, for instance in the  $q\bar{q} \rightarrow b\bar{b}H$  process.





## Acknowledgements

First of all, I would like to thank Prof. Dr. Tilman Plehn for giving me the opportunity to work on such an intriguing topic at the frontiers of science. It was a pleasure to work and discuss with you and I thank you for being so available to answer all my questions while giving me a lot of space to develop my own ideas. I owe a special thanks to Anke Biekötter and Jennifer Thompson for always answering my questions, be it related to physics or to computing. Without your advice, some event samples and your proof-reading this thesis would not be what it is. Susanne Westhoff also deserves a big thank you for some final advice and proof-reading. Finally, the entire research group for New Physics at the LHC deserves a big thank you for providing such a friendly, cooperative and truly inspiring environment.

# References

- [1] S. Schael *et al.* [ALEPH and DELPHI and L3 and OPAL and SLD Collaborations and LEP Electroweak Working Group and SLD Electroweak Group and SLD Heavy Flavour Group], Phys. Rept. **427** (2006) 257 doi:10.1016/j.physrep.2005.12.006 [hep-ex/0509008].
- [2] J. H. Oort, Bulletin of the Astronomical Institutes of the Netherlands, 4, 249 (1932); F. Zwicky, Helv. Phys. Acta. 6, 110-127 (1933); F. Zwicky. Ap.J. 86 217-246 (1937).
- [3] S. O. Bilson-Thompson, F. Markopoulou and L. Smolin, Class. Quant. Grav. 24:3975-3994, (2007) [arXiv:hep-th/0603022v2]; A. H. Chamseddine, A. Connes and M. Marcolli, Adv. Theor. Math. Phys. 11:991-1089 (2007) [arXiv:hep-th/0610241v1].
- [4] C. Englert, T. Plehn, D. Zerwas and P. M. Zerwas, Phys. Lett. B 703:298-305, 2011. [arXiv:1106.3097v2].
- [5] S. Dittmaier *et al.*, doi:10.5170/CERN-2011-002 [arXiv:1101.0593 [hep-ph]]; S. Dittmaier *et al.*, doi:10.5170/CERN-2012-002, [arXiv:1201.3084 [hep-ph]].
- [6] T. Plehn, *Lectures on LHC Physics*, Lecture notes in Physics, volume 886, Springer, Berlin, Heidelberg [u.a.], 2. ed., 2015.
- [7] O. J. P. Eboli and D. Zeppenfeld, Phys. Lett. B **495** (2000) 147 doi:10.1016/S0370-2693(00)01213-2 [hep-ph/0009158].
- [8] D. J. Griffiths, *Introduction to Elementary Particles*, Wiley-VCH, Weinheim, 2. rev. ed. edition, 2008.
- [9] A. Bettini, *Introduction to Elementary Particle Physics*, Cambridge University Press, Cambridge, 2008.

- [10] M. D. Schwartz, *Quantum Field Theory and the Standard Model*, Cambridge University Press, Cambridge [u.a.], 2014.
- [11] M. Srednicki, *Quantum Field Theory*, Cambridge University Press, Cambridge [u.a.], 2007.
- [12] F. Englert and R. Brout, *Phys. Rev. Lett.* **13** (1964) 321. doi:10.1103/PhysRevLett.13.321; P. W. Higgs, *Phys. Lett.* **12** (1964) 132. doi:10.1016/0031-9163(64)91136-9; G. S. Guralnik, C. R. Hagen and T. W. B. Kibble, *Phys. Rev. Lett.* **13** (1964) 585. doi:10.1103/PhysRevLett.13.585; P. W. Higgs, *Phys. Rev.* **145** (1966) 1156. doi:10.1103/PhysRev.145.1156; T. W. B. Kibble, *Phys. Rev.* **155** (1967) 1554. doi:10.1103/PhysRev.155.1554
- [13] E. Corbelli and P. Salucci, *Mon. Not. Roy. Astron. Soc.* **311** (2000) 441 doi:10.1046/j.1365-8711.2000.03075.x [astro-ph/9909252].
- [14] R. Aaij *et al.* [LHCb Collaboration], arXiv:1704.08217 [hep-ex].
- [15] V. Barger and R. Philips, *Collider Physics. Frontiers in Physics. Physics Textbook*, volume 71, Addison-Wesley Publishing, Reading, Massachusetts, updated ed. edition, 1997.
- [16] R. K. Ellis, J. Stirling and B. R. Webber, *QCD and Collider Physics*, Cambridge University Press, Caellismbridge [u.a.], 1996.
- [17] J. de Favereau *et al.* [DELPHES 3 Collaboration], *JHEP* **1402** (2014) 057 doi:10.1007/JHEP02(2014)057 [arXiv:1307.6346 [hep-ex]].
- [18] J. Alwall, M. Herquet, F. Maltoni, O. Mattelaer and T. Stelzer, *JHEP* **1106** (2011) 128 doi:10.1007/JHEP06(2011)128 [arXiv:1106.0522 [hep-ph]].

- [19] T. Sjostrand, S. Mrenna and P. Z. Skands, JHEP **0605** (2006) 026 doi:10.1088/1126-6708/2006/05/026 [hep-ph/0603175].
- [20] E. Conte, B. Fuks and G. Serret, Comput. Phys. Commun. **184** (2013) 222 doi:10.1016/j.cpc.2012.09.009 [arXiv:1206.1599 [hep-ph]].
- [21] T. Ohl, Comput. Phys. Commun. **90** (1995) 340 doi:10.1016/0010-4655(95)90137-S [hep-ph/9505351].
- [22] G. Aad *et al.* [ATLAS Collaboration], JHEP **1601** (2016) 172 doi:10.1007/JHEP01(2016)172 [arXiv:1508.07869 [hep-ex]].
- [23] C. P. Burgess and G. D. Moore, *The Standard Model*, Cambridge University Press, Cambridge [u.a.], 2013.
- [24] V. Khachatryan *et al.* [CMS Collaboration], JHEP **1702** (2017) 135 doi:10.1007/JHEP02(2017)135 [arXiv:1610.09218 [hep-ex]].
- [25] C. Bernaciak, T. Plehn, P. Schichtel and J. Tattersall, Phys. Rev. D **91** (2015) 035024 doi:10.1103/PhysRevD.91.035024 [arXiv:1411.7699 [hep-ph]].
- [26] R. M. Godbole, M. Guchait, K. Mazumdar, S. Moretti and D. P. Roy, Phys. Lett. B **571** (2003) 184 doi:10.1016/j.physletb.2003.06.066 [hep-ph/0304137].
- [27] G. Aad *et al.* [ATLAS Collaboration], Phys. Rev. Lett. **112** (2014) 201802 doi:10.1103/PhysRevLett.112.201802 [arXiv:1402.3244 [hep-ex]].
- [28] S. Chatrchyan *et al.* [CMS Collaboration], Eur. Phys. J. C **74** (2014) 2980 doi:10.1140/epjc/s10052-014-2980-6 [arXiv:1404.1344 [hep-ex]].
- [29] T. Gleisberg, S. Hoeche, F. Krauss, M. Schonherr, S. Schumann, F. Siegert and J. Winter, JHEP **0902** (2009) 007 doi:10.1088/1126-6708/2009/02/007 [arXiv:0811.4622 [hep-ph]].

- [30] R. Brun and F. Rademakers, Nucl. Instrum. Meth. A **389** (1997) 81. doi:10.1016/S0168-9002(97)00048-X.
- [31] L. Garren, F. Krauss, C.-J. Lin, S. Navas, P. Richardson and T. Sjöstrand, 43. *Monte Carlo Numbering Scheme*. <http://pdg.lbl.gov/2016/reviews/rpp2016-rev-monte-carlo-numbering.pdf>, 2016.
- [32] F. Cascioli *et al.*, Phys. Lett. B **735** (2014) 311 doi:10.1016/j.physletb.2014.06.056 [arXiv:1405.2219 [hep-ph]].
- [33] A. D. Martin, W. J. Stirling, R. S. Thorne and G. Watt, Eur. Phys. J. C **63** (2009) 189 doi:10.1140/epjc/s10052-009-1072-5 [arXiv:0901.0002 [hep-ph]].
- [34] A. Hocker *et al.*, PoS ACAT (2007) 040 [physics/0703039 [PHYSICS]].
- [35] Baden-Württemberg's HPC Services (BwUniCluster). The author acknowledges support by the state of Baden-Württemberg through HPC. <https://www.bwhpc-c5.de/wiki/index.php/Category:BwUniCluster>.
- [36] H. L. Lai, J. Huston, S. Mrenna, P. Nadolsky, D. Stump, W. K. Tung and C.-P. Yuan, JHEP **1004** (2010) 035 doi:10.1007/JHEP04(2010)035 [arXiv:0910.4183 [hep-ph]].
- [37] LHC Higgs Cross Section Working Group, [https://twiki.cern.ch/twiki/bin/view/LHCPhysics/CERNYellowReportPageAt13TeV#ZH\\_Process](https://twiki.cern.ch/twiki/bin/view/LHCPhysics/CERNYellowReportPageAt13TeV#ZH_Process)
- [38] M. Grazzini, S. Kallweit, D. Rathlev and M. Wiesemann, Phys. Lett. B **761**, 179 (2016) doi:10.1016/j.physletb.2016.08.017 [arXiv:1604.08576 [hep-ph]].
- [39] T. Gehrmann, M. Grazzini, S. Kallweit, P. Maierhofer, A. von Manteuffel,

S. Pozzorini, D. Rathlev and L. Tancredi, Phys. Rev. Lett. **113**, no. 21, 212001 (2014) doi:10.1103/PhysRevLett.113.212001 [arXiv:1408.5243 [hep-ph]].

[40] M. Czakon and A. Mitov, Comput. Phys. Commun. **185**, 2930 (2014) doi:10.1016/j.cpc.2014.06.021 [arXiv:1112.5675 [hep-ph]]; [https://twiki.cern.ch/twiki/bin/view/LHCPhysics/TtbarNNLO#Top\\_quark\\_pair\\_cross\\_sections\\_at](https://twiki.cern.ch/twiki/bin/view/LHCPhysics/TtbarNNLO#Top_quark_pair_cross_sections_at)

[41] Wolfram Research, Inc., Mathematica, Version 10.2, Champaign, IL (2015).

# Erklärung

Ich versichere, dass ich diese Arbeit selbstständig verfasst und keine anderen als die angegebenen Quellen und Hilfsmittel benutzt habe.

Heidelberg, der 06. Juni 2017,

Rhea Moutafis